Supplementary Material
Leveraging the Availability of Two Cameras for Illuminant Estimation

Abdelrahman Abdelhamed Abhijith Punnappurath Michael S. Brown
Samsung AI Center – Toronto
{a.abdelhamed,abhijith.p,michael.b1}@samsung.com

This supplementary material contains additional experiments and details that could not be included in the main paper due to space constraints.

S1. Predicting the second camera illuminant

In the main paper, we had focused on estimating scene illuminants for the first camera. In this experiment, we train the same models, described in the main paper, to predict the illuminants for the second camera. Table S1 shows the results for estimating illuminants for the second camera on our radiometric dataset. As discussed in the main paper, our method works well, and it yields the best results for predicting illuminants for the second camera too. Table S2 shows the results for the second camera on the S20 real dataset. It can be observed that our method performs well in comparison with the state-of-the-art. Note that although some of the bias correction methods such as [9, 2] produce a lower error on the best 25%, their worst 25% performance is very poor compared to our method indicating that their overall fit is quite poor. The FC4 [13] deep net, our closest competitor, reports a slightly better Q3, but has orders of magnitude more parameters than our method. We noticed that our accuracy is lower on the second camera compared to the main camera, but only very slightly so. This difference may be due to variations in sensitivity between the two sensors, or the training heuristics between the two trained models.

Method	Mean	Med	B25%	W25%	Q1	Q3
GW [6]	3.40	3.04	1.15	6.24	1.81	4.63
SoG [10]	3.76	3.29	1.26	7.02	2.01	5.08
GE-1 [16]	4.26	3.79	1.34	7.99	2.18	5.79
GE-2 [16]	4.44	3.86	1.44	8.42	2.33	6.09
WGE [12]	3.58	2.68	0.95	7.76	1.52	4.57
PCA [7]	3.72	2.35	0.93	8.83	1.37	4.73
WP [5]	4.65	4.15	1.51	8.68	2.43	6.39
Gamut Pixel [11]	3.10	2.52	0.94	6.22	1.46	4.24
Gamut Edge [11]	5.34	4.70	1.73	10.02	2.79	7.30
Ours (200 params)	2.39	1.85	0.58	5.12	0.99	3.28
Ours (470 params)	**2.19**	**1.57**	**0.47**	**4.95**	**0.83**	**2.92**
Ours (1460 params)	2.48	1.82	0.57	5.47	0.96	3.41

Table S1: Angular errors (degrees) on our radiometric dataset for the second camera. Best results are in bold.

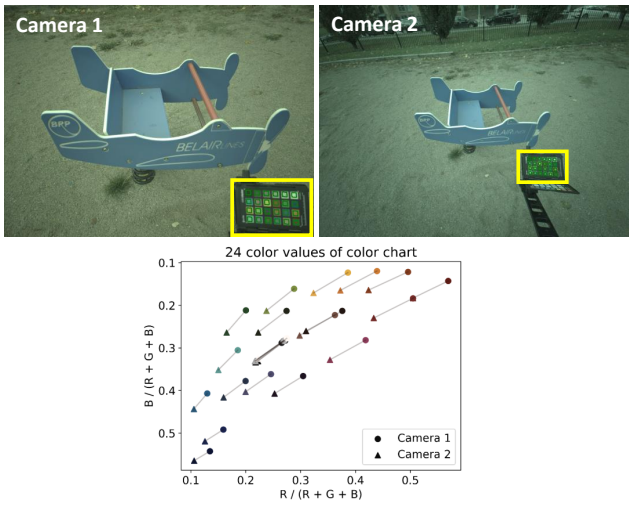

Figure S1: (Top) Two images from the two cameras from our S20 real dataset, captured under the same illumination. (Bottom) A scatter plot showing the differences between the color values of the 24 color chart patches found in each image. This example illustrates the difference in the spectral sensitivity between the two cameras.

S2. Difference in spectral sensitivity between the two cameras

Figure S1 shows the difference in spectral sensitivity between the two cameras used to capture the S20 dataset. The scatter plot shows the differences between the color values of the 24 color chart patches found in two images of the same scene under the same illumination. The clear separation observed between corresponding patches validates our assumption that sensors on real two-camera systems can

Method	Mean	Med	B25%	W25%	Q1	Q3
GW [6]	2.36	1.94	0.56	4.99	0.94	2.99
SoG [10]	2.72	1.89	0.66	6.30	1.00	3.62
GE-1 [16]	5.26	4.14	1.04	11.56	1.50	8.44
GE-2 [16]	5.87	4.07	1.04	13.32	1.60	9.28
WGE [12]	6.77	4.93	1.00	15.34	1.63	11.82
PCA [7]	4.29	2.82	0.82	10.12	1.28	6.16
WP [5]	2.75	2.13	0.53	6.14	1.00	3.43
Gamut Pixel [11]	7.24	6.15	1.32	14.71	2.37	12.73
Gamut Edge [11]	4.90	4.48	0.79	10.46	1.58	7.16
CM [8]	2.92	1.95	0.46	6.65	0.88	4.66
Homography [9] (SoG)	3.94	3.10	**0.34**	9.30	0.65	5.86
Homography [9] (PCA)	3.34	2.70	0.49	6.96	1.02	5.42
APAP [2] (GW)	2.89	2.14	0.37	6.59	0.75	4.52
APAP [2] (SoG)	3.71	2.45	**0.34**	9.08	0.71	5.76
APAP [2] (PCA)	3.16	2.56	0.35	6.82	0.91	4.96
SIIE [1]	4.55	3.77	0.73	9.30	1.41	7.56
Quasi U CC [4]	3.53	2.11	0.68	8.37	1.14	4.81
Quasi U CC finetuned [4]	2.52	1.85	0.59	5.63	0.96	3.34
FC4 [13]	1.95	1.56	0.54	3.91	1.03	**2.44**
FFCC [3]	2.03	1.72	0.59	4.02	0.95	2.67
Ours (200 params)	**1.68**	1.55	0.54	**3.03**	0.72	2.50
Ours (470 params)	1.82	1.71	0.65	3.24	0.89	2.47
Ours (1460 params)	1.75	**1.44**	0.44	3.50	**0.69**	2.61

Table S2: Angular errors (degrees) on the second camera from our S20 two-camera dataset. Best results are in bold.

likely have different spectral profiles in practice.

S3. Experiments on two similar cameras

In the main paper, for the radiometric dataset, we selected two different cameras from two different manufacturers from the dataset of [14]. In this experiment, we select two similar cameras from [14] from the same manufacturer with similar spectral sensitivity functions. Plots of the distribution of ground truth illuminants corresponding

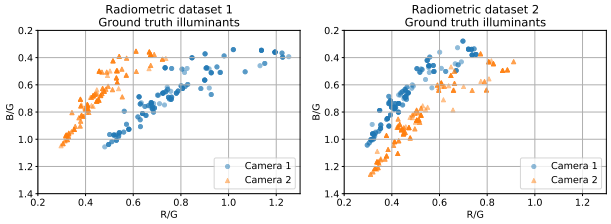

(A) Dissimilar cameras (B) Similar cameras

Figure S2: Plots of ground truth illuminants for the two cameras from our radiometric datasets where (A) the two cameras are from different manufacturers and have different spectral sensitivity profiles, and (B) the two cameras are from the same manufacturer and have very similar spectral characteristics. Note that plot (A) has been reproduced from Fig. 5(A) of the main paper for ease of comparison. It can be observed that the illuminants from the two cameras are grouped closer together in plot (B) because the two cameras have similar spectral sensitivity functions.

to the two cameras for both these datasets are shown in Fig. S2. Tables S3 and S4 show that even with slight differences in the spectral sensitivity between the two cameras, our method still performs well and achieves better results than many well-established single-image methods.

S4. Experiments with larger networks

In this experiment, we train the larger network with 1460 parameters on the radiometric dataset. Table S5 shows the results compared to the other two smaller networks presented in the main paper. The larger network seems to overfit the training data, and hence, yields slightly worse results than the smaller networks. Similar observations can

Method	Mean	Med	B25%	W25%	Q1	Q3
GW [6]	3.57	3.25	1.23	6.47	1.91	4.89
SoG [10]	3.85	3.43	1.29	7.13	2.00	5.23
GE-1 [16]	4.36	3.86	1.42	8.15	2.26	5.98
GE-2 [16]	4.59	3.99	1.47	8.75	2.38	6.18
WGE [12]	3.83	2.85	0.99	8.40	1.61	4.93
PCA [7]	4.08	2.56	0.96	9.72	1.47	5.27
WP [5]	4.70	4.20	1.60	8.69	2.52	6.34
Gamut Pixel [11]	3.21	2.58	0.93	6.48	1.47	4.37
Gamut Edge [11]	5.49	4.88	1.84	10.20	2.90	7.42
Ours (200 params)	3.07	2.41	0.75	6.48	1.28	4.30
Ours (470 params)	**2.57**	**1.81**	**0.43**	**5.97**	**0.82**	**3.63**

Table S3: Angular errors (degrees) on another radiometric dataset where both cameras are from the same manufacturer. The results shown are for the first camera.

Method	Mean	Med	B25%	W25%	Q1	Q3
GW [6]	3.87	3.51	1.30	7.05	2.04	5.33
SoG [10]	4.39	3.93	1.49	8.04	2.36	5.92
GE-1 [16]	4.95	4.40	1.62	9.22	2.56	6.76
GE-2 [16]	5.11	4.43	1.61	9.77	2.57	6.94
WGE [12]	4.15	3.04	1.06	9.14	1.73	5.35
PCA [7]	4.10	2.75	0.97	9.58	1.56	5.12
WP [5]	5.09	4.54	1.71	9.46	2.71	6.88
Gamut Pixel [11]	3.52	2.93	1.01	7.02	1.63	4.82
Gamut Edge [11]	6.01	5.39	2.01	11.09	3.20	8.09
Ours (200 params)	3.27	2.56	0.78	6.96	1.32	4.49
Ours (470 params)	**2.85**	**2.00**	**0.54**	**6.60**	**0.96**	**3.92**

Table S4: Angular errors (degrees) on another radiometric dataset where both cameras are from the same manufacturer. The results shown are for the second camera.

Method	Mean	Med	B25%	W25%	Q1	Q3
Ours (200 params)	2.80	2.20	0.72	5.87	1.19	3.81
Ours (470 params)	**2.65**	**2.00**	**0.64**	**5.72**	**1.07**	**3.61**
Ours (1460 params)	2.90	2.23	0.69	6.23	1.16	4.03

Table S5: Angular errors (degrees) on the radiometric dataset for the first camera using larger network sizes. Best results are in bold.

be made in Table S1. All models were trained with the Adam [15] optimizer for 1 million epochs.

References

[1] Mahmoud Afifi and Michael S. Brown. Sensor-independent illumination estimation for DNN models. In *BMVC*, 2019. 2

[2] Mahmoud Afifi, Abhijith Punnappurath, Graham D. Finlayson, and Michael S. Brown. As-projective-as-possible bias correction for illumination estimation algorithms. *JOSA-A*, 36(1):71–78, 2019. 1, 2

[3] Jonathan T. Barron and Yun-Ta Tsai. Fast fourier color constancy. In *CVPR*, 2017. 2

[4] Simone Bianco and Claudio Cusano. Quasi-unsupervised color constancy. In *CVPR*, 2019. 2

[5] David H. Brainard and Brian A. Wandell. Analysis of the retinex theory of color vision. *JOSA-A*, 3(10):1651–1661, 1986. 1, 2

[6] Gershon Buchsbaum. A spatial processor model for object colour perception. *Journal of the Franklin Institute*, 310(1):1 – 26, 1980. 1, 2

[7] Dongliang Cheng, Dilip K. Prasad, and Michael S. Brown. Illuminant estimation for color constancy: Why spatial-domain methods work and the role of the color distribution. *JOSA-A*, 31(5):1049–1058, 2014. 1, 2

[8] Graham D. Finlayson. Corrected-moment illuminant estimation. In *ICCV*, 2013. 2

[9] Graham D. Finlayson. Colour and illumination in computer vision. *Interface Focus*, 8, 2018. 1, 2

[10] Graham D. Finlayson and Elisabetta Trezzi. Shades of gray and colour constancy. In *Color Imaging Conference*, 2004. 1, 2

[11] Arjan Gijsenij, Theo Gevers, and Joost Van De Weijer. Generalized gamut mapping using image derivative structures for color constancy. *IJCV*, 86:127–139, 2008. 1, 2

[12] Arjan Gijsenij, Theo Gevers, and Joost Van De Weijer. Improving color constancy by photometric edge weighting. *TPAMI*, 34(5):918–929, 2012. 1, 2

[13] Yuanming Hu, Baoyuan Wang, and Stephen S Lin. FC4: Fully convolutional color constancy with confidence-weighted pooling. In *CVPR*, 2017. 1, 2

[14] Jun Jiang, Dengyu Liu, Jinwei Gu, and Sabine Süsstrunk. What is the space of spectral sensitivity functions for digital color cameras? In *WACV*, 2013. 2

[15] Diederik P. Kingma and Jimmy Ba. Adam: A method for stochastic optimization. *ICLR*, 2014. 3

[16] Joost Van De Weijer, Theo Gevers, and Arjan Gijsenij. Edge-based color constancy. *TIP*, 16(9), 2007. 1, 2